Characteristics and surface analysis of ion beam deposition from binary boron platinum ($Pt_{58}B_{42}$) liquid-metal ion source

R. H. Higuchi-Rusli, J. C. Corelli, A. J. Steckl, and H-S. Jin
Center for Integrated Electronics, Rensselaer Polytechnic Institute, Troy, New York 12181

(Received 14 November 1986; accepted for publication 21 September 1987)

Characteristics of a eutectic boron platinum ($Pt_{58}B_{42}$) liquid-metal ion source (LMIS) were analyzed and investigated with a quadrupole mass spectrometer (QMS), Auger electron spectroscopy (AES), and Rutherford backscattering spectroscopy (RBS). The source characteristics can be explained by the hydrodynamic model, particularly for needle geometry LMIS. Surface analysis with RBS and AES indicated that more boron is produced in the ion beam than left in the liquid alloy reservoir and more droplets are produced with a 10-μm emitter tip radius, which reduced boron current in the beam. The source instability was associated with droplet formation. AES results show that substantial neutral ions were produced which was not detected by QMS. RBS results on the depleted residual alloy remaining on the carbon ribbon heater indicated that the cause of the alloy system's short lifetime (33 h) is due to a change in alloy stoichiometry to a higher platinum content. Three different emitter tip radii (2.5, 5, and 10 μm) made of graphite were used in the present investigation. Higher boron current and high stability during ion emission was recorded with 2.5-μm graphite emitter tip radius than with the 5- or 10-μm tip radii.

I. INTRODUCTION

A considerable number of papers have been published dealing with the application of liquid-metal ion sources (LMIS) in the focused ion beam (FIB) system. The liquid-metal ion source is used as a primary source for submicron level fabrication of IC devices.[1–5] In the FIB system, a LMIS is used as a high brightness source for a variety of purposes such as direct write dopant sources, micromachining, and photomask repair. Among these ion sources and their applications, the boron source is the most difficult one to fabricate because of its higher melting temperature and associated metallurgical problems. A variety of boron alloys have been tested as possible boron sources in the FIB system.[6–8] The binary eutectic of $Pt_{58}B_{42}$ was selected for study in this work because of higher boron content in the alloy and relatively low melting temperature (940 °C) compared to the other boron sources.[6]

Preliminary wetting test results indicate that $Pt_{58}B_{42}$ alloy readily attacks almost any metallic substrate which makes it more difficult to study source characteristics with simple hairpin-type LMIS.[9] Although metallurgically it is less desirable to use this kind of alloy source as a boron source, it is worthwhile to examine its characteristics before a conclusion regarding its usefulness can be made. Additionally, it is worthwhile to examine to what extent the problem associated with this alloy source can be tolerated for FIB application, by taking into consideration all criteria associated with this alloy source. For further investigation of $Pt_{58}B_{42}$ characteristics, it is important first to outline the criteria for an ideal boron alloy source. A boron-producing alloy source must possess at least seven requirements such as: (1) low melting temperature, (2) low vapor pressure, (3) more percent of boron produced in the beam than left in the alloy, (4) long operating lifetime at least greater than 100 h, (5) the source must not become alloyed with the substrate, (6) high stability of $^{11}B^+$ current, and (7) alloy sources must be of the binary type.

A good candidate for a boron-producing alloy source must satisfy at least five of the seven requirements as just outlined. Since the $Pt_{58}B_{42}$ alloy source has already met four of the seven requirements, we therefore report on the remaining criteria such as percent of boron in the beam, source lifetime, and source stability. We also report on the effect of emitter tip radius on the source characteristics from the hydrodynamic point of view.

II. DUAL CARBON FILAMENT LIQUID-METAL ION SOURCE

The boron LMIS design, shown in Fig. 1, is known as a dual carbon filament liquid-metal ion source. The source was built and developed at the CIE-RPI laboratory and consists of a 10-kV, 15-A, three-wire electrical feedthrough on a $2\frac{3}{4}$-in. CF flange with a ceramic (MACOR) insulator.[9] This type of LMIS incorporated two graphite ribbon filaments instead of one and has been tested for its reliability with a $Pd_{73}B_{27}$ alloy for more than 120 h.[7] Two graphite ribbon filaments are more stable than a single graphite ribbon filament and provide a stable liquid-metal flow from reservoir to the emitter tip. For the $Pt_{58}B_{42}$ boron-producing alloy, a silicon-coated graphite emitter was used exclusively because of intolerable metallurgical characteristics of this alloy to dissolve almost all refractory metallic emitter substrates. The graphite emitter needle is anchored in the upper graphite ribbon filament. The graphite emitter needles were sharpened to 2.5, 5.0, and 10 μm by mechanical grinding and by flame etching.

The alloy, in the form of a small "lump" of 2 mm^3 size, was loaded by inserting between the graphite ribbons at room temperature and atmospheric pressure, followed by melting in vacuum at 10^{-7} Torr to wet the needle. A typical

 0021-8979/88/030878-09$02.40

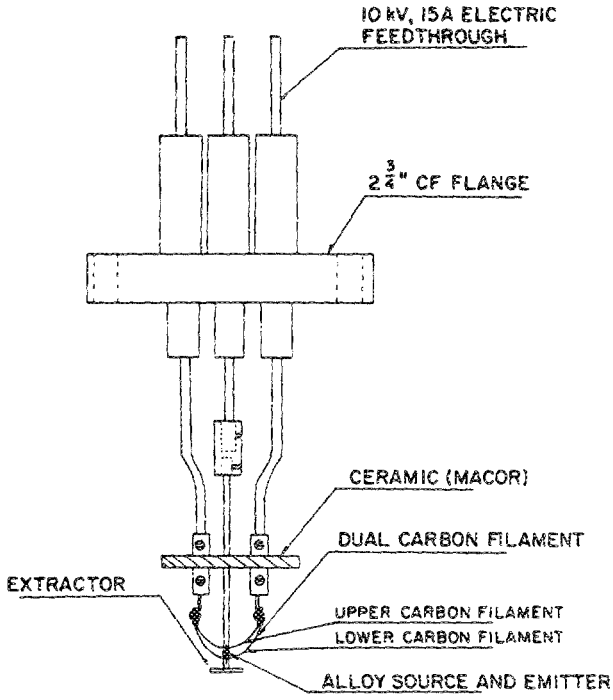

FIG. 1. Dual carbon liquid-metal ion source.

input heater power in the range of 50–80 W was required to melt the alloy and maintain the liquid flow to the emitter tip.

III. RESULTS AND DISCUSSION

A. Binary boron platinum ($Pt_{58}B_{42}$) LMIS characteristics

Figures 2–4 show current-voltage characteristics for three different emitter tips of 2.5, 5.0, and 10 μm radii. The threshold voltage and the ion current at the threshold voltage increases with emitter tip radius, and the slope (dI/dV)

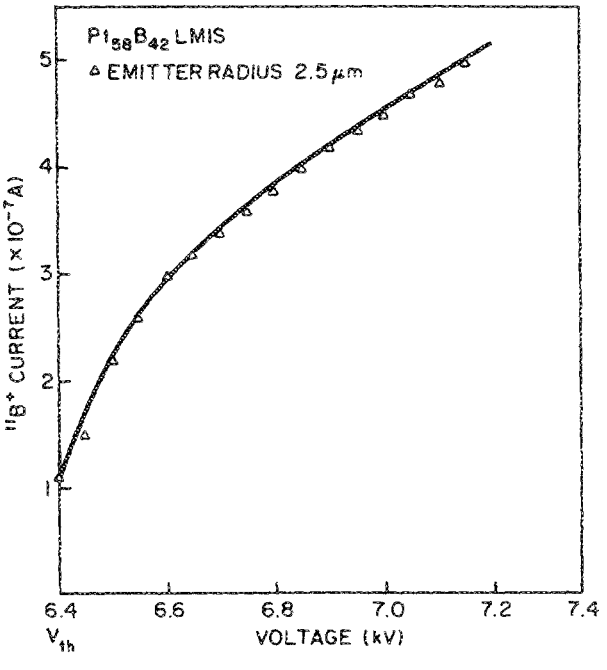

FIG. 2. Current-voltage characteristics of $Pt_{58}B_{42}$ LMIS for 2.5-μm emitter.

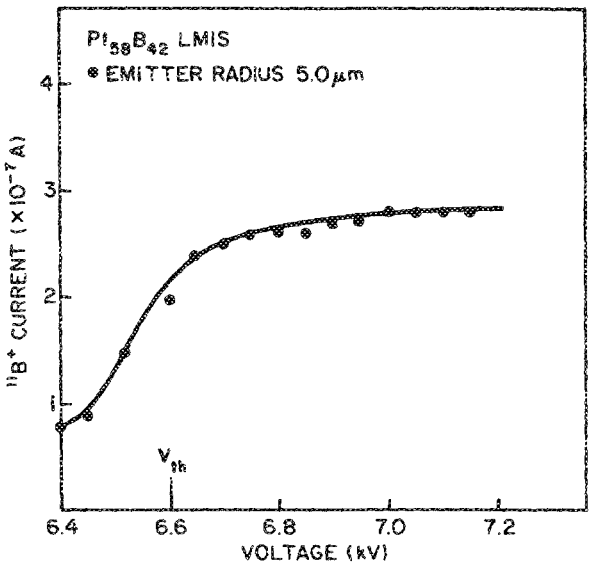

FIG. 3. Current-voltage characteristics of $Pt_{58}B_{42}$ LMIS for 5.0-μm emitter.

at the threshold voltage also increases with emitter tip radius. A similar characteristic has been reported for a liquid-gold ion source which suggests that ion emission is not controlled by space-charge effects but rather is determined by liquid flow impedance along the needle emitter.[10,11] In other words, if the space-charge effects at the apex of the Taylor cone limit the ion emission rate, the I-V characteristics would not depend on the geometry of the needle, and universal I-V curves would be observed.[11] The experimental current-voltage characteristics presented in this paper basically agree with the calculations given in Ref. 11. The calculations[11] do not predict the magnitude of the emitted ion current which depends on the emitter tip radius as observed here. [See Figs. 5(a)–5(c).]

Figures 5(a) and 5(b) show current-time measurements for two different emitter tip radii at constant applied

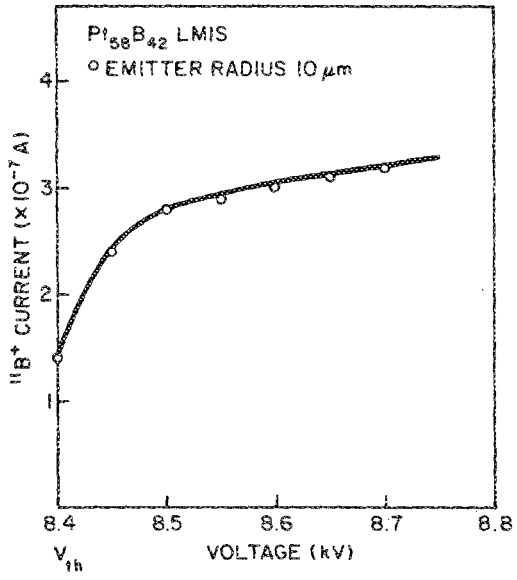

FIG. 4. Current-voltage characteristics of $Pt_{58}B_{42}$ LMIS for 10-μm emitter.

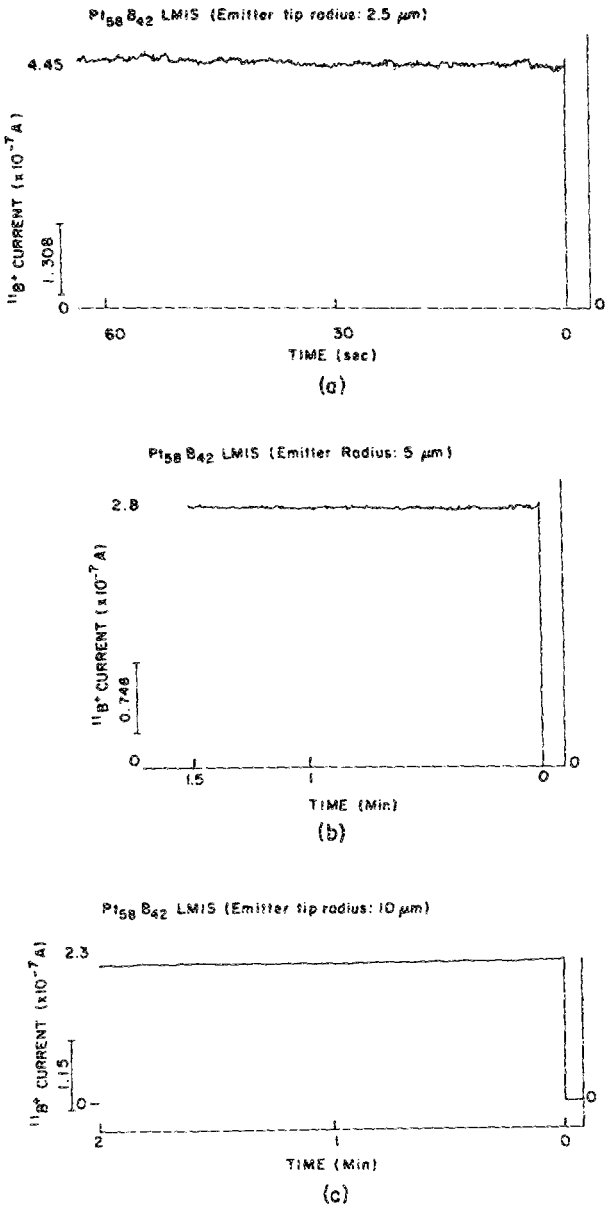

FIG. 5. $^{11}B^+$ current vs time measurement of $Pt_{58}B_{42}$ LMIS recorded (a) for 2.5-μm emitter tip radius after 33-h test run, (b) for 5.0-μm emitter tip radius after 2-h test run, (c) for 10-μm emitter tip radius after 2-h test run.

voltage (7 keV). The large current drift (6%) was observed with 2.5-μm emitter tip, but the recorded boron $^{11}B^+$ current is higher compared to the two other emitter tip radii (5 and 10 μm). The lower boron current recorded with 5- and 10-μm emitter tip radii suggests that a substantial number of neutral atoms and droplets must have formed during emission, which reduces the amount of $^{11}B^+$ current in the beam. The drift and decrease in $^{11}B^+$ current is shown more clearly by recording a repeat spectrum of $^{11}B^+$ with time up to 15 min. The recorded $^{11}B^+$ current variation with time for both 2.5- and 5.0-μm emitter tip radii are shown more clearly in Figs. 6(a) and 6(b). The variation in current is caused by liquid-metal flow impedance such as mass flowrate, Taylor cone apex radius, and changes in the effective liquid-film thickness. This result was well explained with the hydrodynamic model of Ga LMIS proposed earlier,[11] and may be the

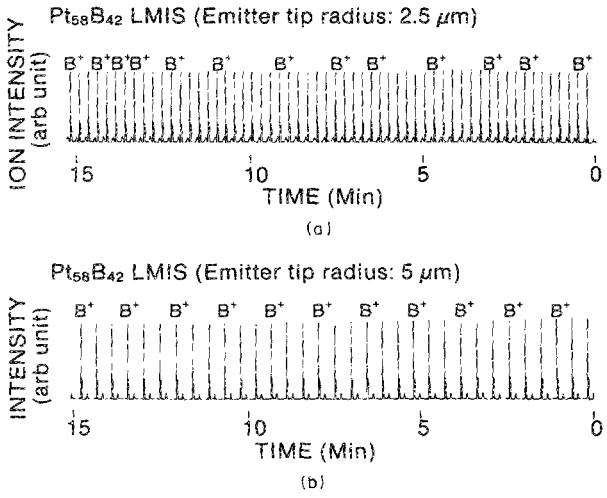

FIG. 6. Repeat scanning of $Pt_{58}B_{42}$ LMIS mass spectrum recorded (a) for 2.5-μm emitter tip radius after 8-h test run, (b) for 5.0-μm emitter tip radius after 8-h test run.

reason for the steep slope of $^{11}B^+$ current-voltage characteristics shown in Fig. 2, which causes larger current drift [see Fig. 5(a)]. The hydrodynamics limitation was evident from reports of extremely steep I-V curves (large dI/dV) observed for nozzle geometry ion sources,[12] and suggests that although the stability depends on the hydrodynamic factors of flow of liquid metal to the emitter tip, the emitter radius does play an important role in the magnitude of current emission. The result is shown in Fig. 7 measured with a 250-μm retractable aperture in front of the beam path. Lower current density was recorded with larger emitter tip radius due to droplets and neutral emissions. Figure 8 shows a long-term stability measurement of $^{11}B^+$ current at constant applied voltage for three different emitter tip radii. The source lifetime and stability are the most important critical measurements on source characteristics and operating proper-

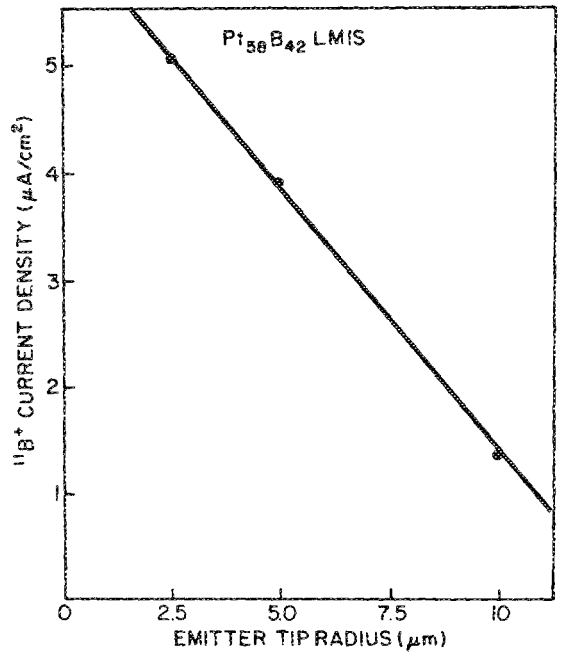

FIG. 7. $^{11}B^+$ LMIS current density vs emitter tip radius.

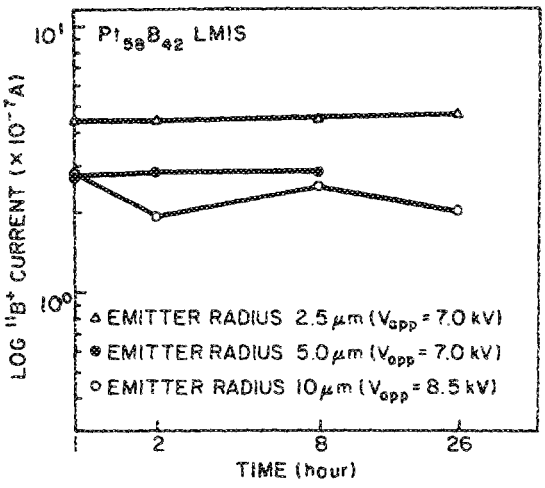

FIG. 8. Long-term stability measurement of $^{11}B^+$ current for different emitter tip radii.

ties. Therefore, although short-term stability measurements may appear encouraging, this alone does not define the overall performance of LMIS for FIB applications.

From long-term stability results, we observed very stable $^{11}B^+$ current recorded with a 2.5-μm radius tip up to 26 h. The $^{11}B^+$ current drift during its lifetime is less than 2%. Hence, adding to the model for reducing the ion energy spread in the LMIS, as suggested earlier[11] for focused ion beam applications, one must be more concerned about the formation of droplets and neutral atoms in the beam by varying emitter tip radius in order to produce lower current density at the target (wafer), as suggested in Ref. 11, to minimize chromatic aberration. In other words, lowering flow impedance by increasing the emitter tip radius would not be a good approach to minimize current density in order to achieve lower chromatic aberration, since this causes more droplets and neutral atoms to be produced. The experimental evidence which supports the concept of lowering chromatic aberration by reducing current density at the target (wafer) has been reported for sources operating at a series of temperatures.[13] The evidence suggests that as the temperature was decreased, the energy spread decreased which was attributed in Ref. 11 to an increase in surface tension and viscosity with decreasing temperature. The results obtained with binary boron platinum ($Pt_{58}B_{42}$) agree with the general guideline given in Ref. 11, that is, to have minimum energy spread for a given liquid metal one must have (1) current as low as possible, (2) temperature as low as possible, and (3) the needle must have a small radius and smooth surfaces.

TABLE I. $Pt_{58}B_{42}$ LMIS current and lifetime measured by quadrupole mass spectrometer.

Tip radius (μm)	Lifetime (h)	Current ($10^{-1}\mu$A) $I_{B^{11}}$	Current ($10^{-1}\mu$A) I_T	Charge (10^{-3} C)
2.5	26	4.45	9.07	41.6
5.0	8	2.76	6.83	7.95
10	26	2.30	5.45	21.5

TABLE II. Average $Pt_{58}B_{42}$ LMIS current ratio measured by quadrupole mass spectrometer.

Tip radius (μm)	Beam current ratio (%) $\frac{I_{B^{10}}}{I_{B^{11}}}$	$\frac{I_{B^{10}}}{I_{Tot}}$	$\frac{I_{B^{11}}}{I_{Tot}}$	$\frac{I_{B^{10}}}{I_{B^{10}}+I_{B^{11}}}$
2.5	28	13.78	49.1	21.9
5.0[a]	25.4	10.2	40.4	20.2
10.0	30.4	12.8	42.2	23.3

[a] $I_{B^{++}}/I_{B^+} = 2.9\%$.

Table I summarizes the results obtained with three different emitter tip radii. A lifetime of 26 h was recorded for both 2.5- and 10-μm emitter tip radii, except for 5.0-μm emitter tip which ceased operating in a lifetime test by mechanical failure. The average $^{11}B^+$ current recorded for both 2.5- and 10-μm emitter tip radii are 0.44 and 0.23 μA, respectively. Table II tabulates relative percent abundance of boron isotope ratio and the ratio of isotopes with the total current. Table III tabulates the $^{11}B^+$ current for three emitter tip radii measured directly from the source as well as through a small aperture of 250 μm. The current density and brightness were calculated by first assuming that the virtual source emitting area is a cusp formed from a protruded Taylor cone, which is in the order of 100 times less than the actual emitter tip radius, which is a reasonable assumption based upon evidence observed with transmission electron microscope (TEM).[14,15] Under this assumption, the solid angle can be calculated and gives the value 7.8×10^{-3} rad. By knowing the solid angle and current density, the brightness for each source can be calculated. The result shows that higher brightness and stability occurs with smaller emitter tip radius. Further analysis of the presence of droplets and neutral atoms is given in Sec. III B on mass spectroscopy and surface analysis of LMIS.

B. Mass spectrum and surface analysis of ion beam deposit

A typical mass spectrum of $Pt_{58}B_{42}$ LMIS recorded after an 8-h test run is shown in Fig. 9(a). The emitter tip radius is 2.5 μm, the scan width is set at 140 amu with a scan rate of 1 amu/s. The $^{28}Si^+$ and $^{28}Si^{++}$ appear in the spec-

TABLE III. $Pt_{58}B_{42}$ LMIS current measured by quadrupole mass spectrometer.

Tip radius (μm)	Current[b] (10^{-9} A) $I_{B^{11}}$	Current[b] (10^{-9} A) $I_{B^{11}}$[a]	Current density[b] (10^{-6} A/cm^2) $J_{B^{11}}$	Brightness[b] (10^5 A/cm^2/sr) $B_{r^{11}B^+}$
2.5	445	2.5	5.09	6.64
5.0	276	1.93	3.94	1.28
10.0	230	0.67	1.37	0.11

[a] Current measured with a 250-μm retractable aperture.
[b] Assumed that the virtual source cusp emitting area is 100 times less than the tip radius. This gives calculated solid angle of 7.81×10^{-3} rad.

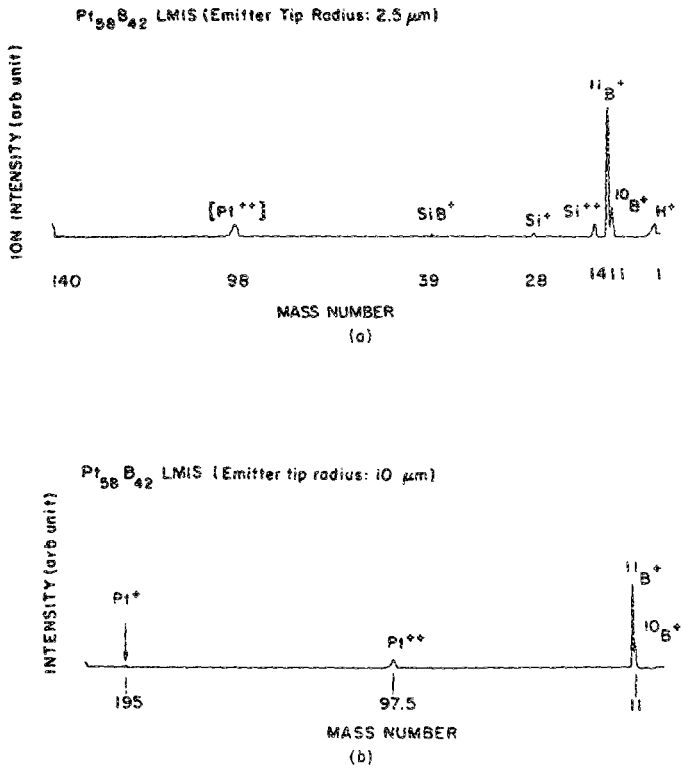

FIG. 9. Mass spectrum of $Pt_{58}B_{42}$ LMIS recorded (a) for 2.5-μm emitter tip radius after 8-h test run, (b) for 5.0-μm emitter tip radius after 20-h test run.

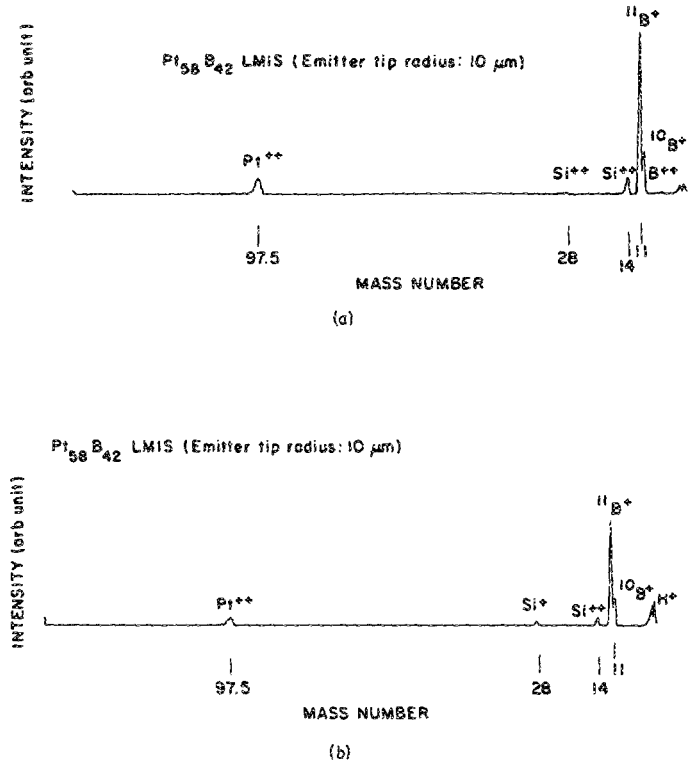

FIG. 10. Mass spectrum of $Pt_{58}B_{42}$ LMIS recorded for 10-μm emitter tip radius (a) after 2-h test run, (b) after 26-h test run.

trum as a result of coating the graphite emitter with silicon to promote wetting between the $Pt_{58}B_{42}$ liquid alloy and the graphite emitter. The boron isotopic ratio shown in Fig. 9(a) is quite close and consistent with the known natural boron isotope abundance ratio. A slight peak height variation of $^{11}B^+$ and $^{10}B^+$ does occur with different emitter tip radii after more than a 20-h test run which might be due to a variation in energy spread. Figure 9(b) shows a mass spectrum of $Pt_{58}B_{42}$ LMIS taken after a 20-h test run. The scanning width in this spectrum was set at 210 amu on the monitor screen, and the scanning rate was set at 1 amu/s. One can notice that the peak intensity of singly ionized platinum [Fig. 9(b)] is quite low when compared to the peak intensity of doubly ionized platinum. The most probable reason for this is due to a different charge of ions and different numbers of secondary electrons produced in the electron multiplier. Even ions of the same mass and charge ratio may produce a different number of secondary electrons in striking the first dynode, and hence, will give different current peak height. Formation of neutral platinum may also contribute to lower Pt^+ current in the beam, and more platinum in the liquid alloy. Silicon singly and doubly ionized ions were not observed due to an expanded horizontal scale which reduces the recorder sensitivity. Figures 10(a) and 10(b) show a similar spectrum for a 10-μm emitter tip radius at a lower scanning width of 140 amu taken after a 2- and 26-h test runs, respectively. An interesting observation to mention here is that the peak intensity of singly ionized platinum is low and is very difficult to record after a 26-h test run. The observed peak intensity of singly ionized platinum is almost the same as that shown in Fig. 9(b).

Table IV tabulates various elements detected by the QMS for three emitter tip radii of 2.5, 5.0, and 10 μm, respectively. The average $^{11}B^+$ currents are 0.45, 0.28, and 0.20 μA, and the total currents detected (i.e., addition of all peaks) are 0.93, 0.72, and 0.43 μA, respectively. From the tabulated elements in Table IV, the (B/Pt) beam is larger than the (B/Pt) alloy for those three emitter tip radii, and there is a clear indication that during the test run, more boron ions were produced in the beam than left behind in the liquid-alloy reservoir at the source. Subsequently, more detailed analyses of beam compositions were carried out with RBS. This was done by placing a clean silicon substrate below the source to collect the beam deposit for analysis to verify the stoichiometry ratio of the film deposit with the

TABLE IV. Percent abundance of various elements in beam for Pt-B alloy on carbon emitter measured with quadrupole mass spectrometer.

Elements	Current (10^{-8} A)			Abundance (%)		
$^{10}B^+$	12[a]	7.0[b]	7.0[c]	12.9[a]	9.7[b]	16.3[c]
$^{11}B^+$	45	28	20	48.4	38.9	46.5
B^{++}		1.0			4.1	
Si^{++}	4.0	4.0	4.0	4.3	5.6	9.3
Si^+	3.0	2.0	2.0	3.2	2.8	4.6
SiB^+	2.0	1.0		2.1	1.4	
$^{194}Pt^{++}$	6.0	5.0	4.0	6.4	6.9	9.3
$^{195}Pt^{++}$	9.0	10.0	3.0	9.7	13.9	7.0
$^{196}Pt^{++}$	7.0	10.0	2.0	7.5	13.9	4.6
$^{198}Pt^{++}$	5.0	4.0	1.0	5.4	5.6	2.3

[a] Total beam current is 0.93 μA, emitter tip radius 2.5 μm.
[b] Total beam current is 0.72 μA, emitter tip radius 5.0 μm.
[c] Total beam current is 0.43 μA, emitter tip radius 10.0 μm.

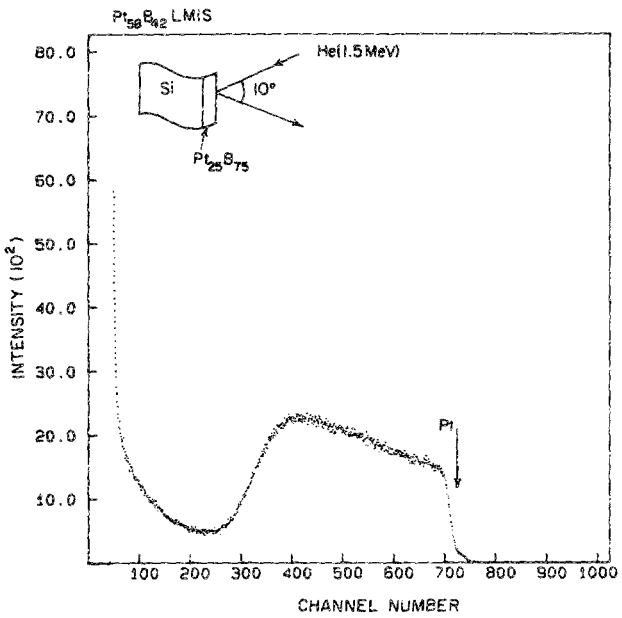

FIG. 11. RBS spectrum of LMIS deposit from 10-μm emitter tip radius at $V_{app} = 8.2$ keV.

stoichiometry ratio in the alloy. Figures 11 and 12 show the RBS results of a deposited film from the B-Pt alloy source. The emitter tip radius was 10 μm. In this analysis, two silicon substrates were used to analyze the stoichiometry of the beam deposit at two different source-applied voltages of 8.2 and 8.5 keV. Two different applied voltages were used to study whether or not there is a significant variation in the stoichiometry ratio between alloy source and film deposit. The calculated stoichiometry ratio of the deposit from RBS resulting after a 3-h deposition are $Pt_{25}B_{75}$ and $Pt_{34}B_{66}$ at applied voltages of 8.2 and 8.5 keV, respectively. These results give additional convincing evidence that more boron is

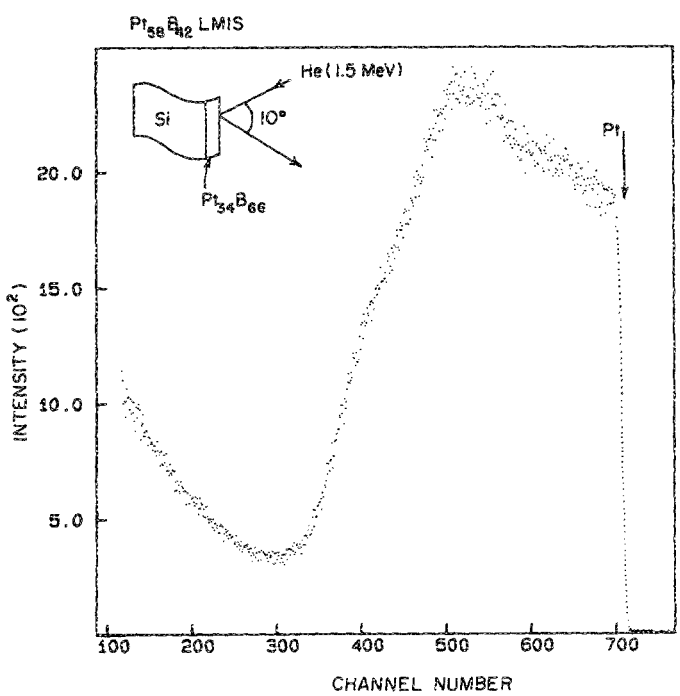

FIG. 12. RBS spectrum of LMIS deposit from 10-μm emitter tip radius at $V_{app} = 8.5$ keV.

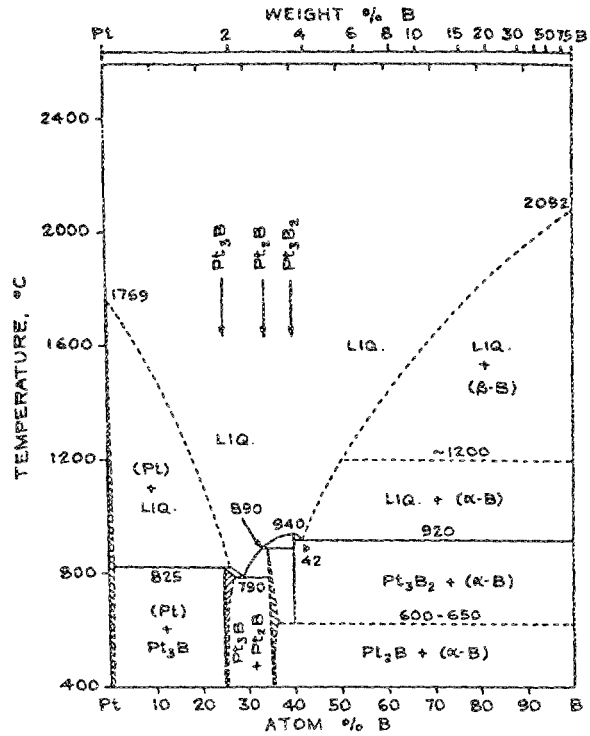

FIG. 13. B-Pt constitution phase diagram (Ref. 15).

produced in the beam than left behind in the liquid-alloy source reservoir. The boron-platinum binary phase diagram is shown in Fig. 13, and gives an approximate phase constituent for these composition ranges of $Pt_{25}B_{75}$ and $Pt_{34}B_{66}$. At 400 °C, these compositions are not stable and exist as two phases of Pt_2B + (alpha-beta). The LMIS had an observed lifetime of 33 h and was recorded on the QMS only up to 26 h. After a 33-h run, the alloy melt ceased to flow from the reservoir to the emitter tip which we believe is due to a change in alloy stoichiometry to a platinum-rich component. The residual alloy in the reservoir was subsequently analyzed with RBS and at the same time, a reference alloy B-Pt (not tested as a liquid-metal source alloy) was analyzed for comparison purposes. Figure 14 shows RBS spectra of both tested and reference samples. The incident ion used is helium at energy $E = 2.0$ MeV. This energy would give a different backscattering energy compared to the previous RBS result of thin-film deposit using 1.5-MeV helium ions. Since the residual deposit is thick, the backscattering energy is small. Notice that the yield of a tested sample in Fig. 14 is much higher than the reference sample which implies a drastic increase in the atomic density of the remaining alloy after a 33-h lifetime test run.

The change in atomic density is due to an increase in platinum content in the alloy which causes liquid metal to cease to flow. The yield of the reference sample is much lower than the tested sample since the helium ion penetrates deeper in the less dense sample. Therefore, the scattered particle suffers an energy loss both in the inward and outward path which is higher than for the dense sample. As a result, the yield with the less dense sample is much lower than for the dense sample. Since boron atoms have a low scattering cross section, most of the scattering yield comes from plati-

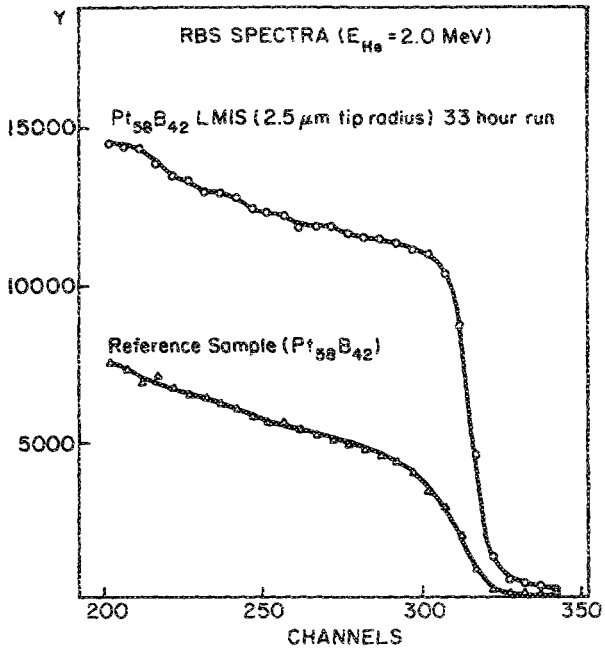

FIG. 14. RBS spectra of reference and depleted $Pt_{58}B_{42}$ LMIS samples.

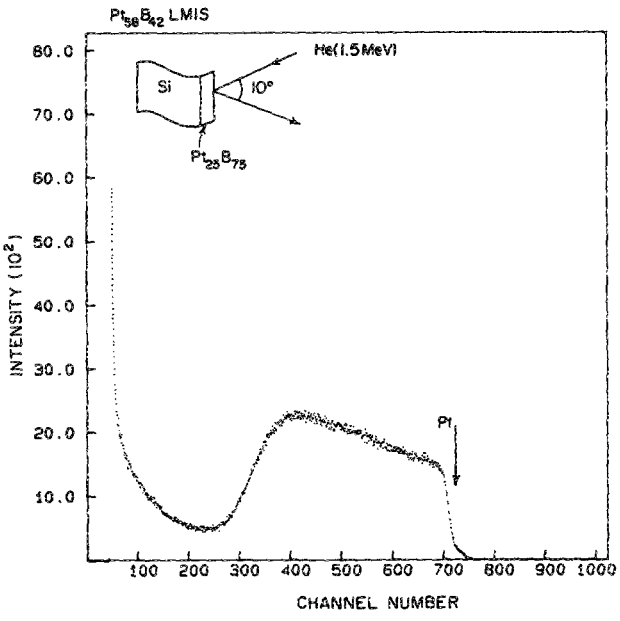

FIG. 15. RBS spectrum of LMIS deposit from 10-μm emitter tip radius at $V_{app} = 8.5$ keV.

num atoms. The RBS analysis provides additional experimental proof of our analysis that more boron is produced in the beam than left behind in the liquid alloy during LMIS operation. This result implies that there has been a change in the alloy stoichiometry to a platinum-rich component with time at source operating temperature, and is the main problem of LMIS with $Pt_{58}B_{42}$ alloy to achieve a 100-h lifetime.

C. Surface analysis of droplets and neutral atom formation

The formation of droplets from indium LMIS has been observed by *in situ* TEM.[14] The TEM observation indicates that when ion emission is initiated, the liquid is drained from the grooves in the tip and substantial liquid flow are required for ion emission. Since the sharp edges of the grooves are exposed, which result in an increase in electric field, the increased electric field stress pulling on the liquid surface tension stress, and results in the formation and growth of the droplets. The droplet formation is not only limited to a grooved emitter needle but can also occur in a polycrystalline needle with grain boundaries. Grain-boundary etching can also occur during LMIS operation forming multidirectional grooves which will initiate droplets. The observation of droplet formation has been reported for both Au and In ion sources and it was suggested that the needle shank is an important site for droplet emission in LMIS.[14]

The droplets can form at the needle shank near the alloy reservoir, and can yield a stoichiometry ratio close to the reservoir alloy composition. Thus, a calculated stoichiometry ratio from RBS results shown in Fig. 15 provides good information about droplet composition which reflects the composition of alloy reservoir. Referring to the phase diagram shown in Fig. 13, this composition is metastable. That is, at 400 °C this composition exists as two phases of platinum-rich (Pt) + Pt_3B. Droplets with this composition can easily occur at 940 °C because at this composition and tem-

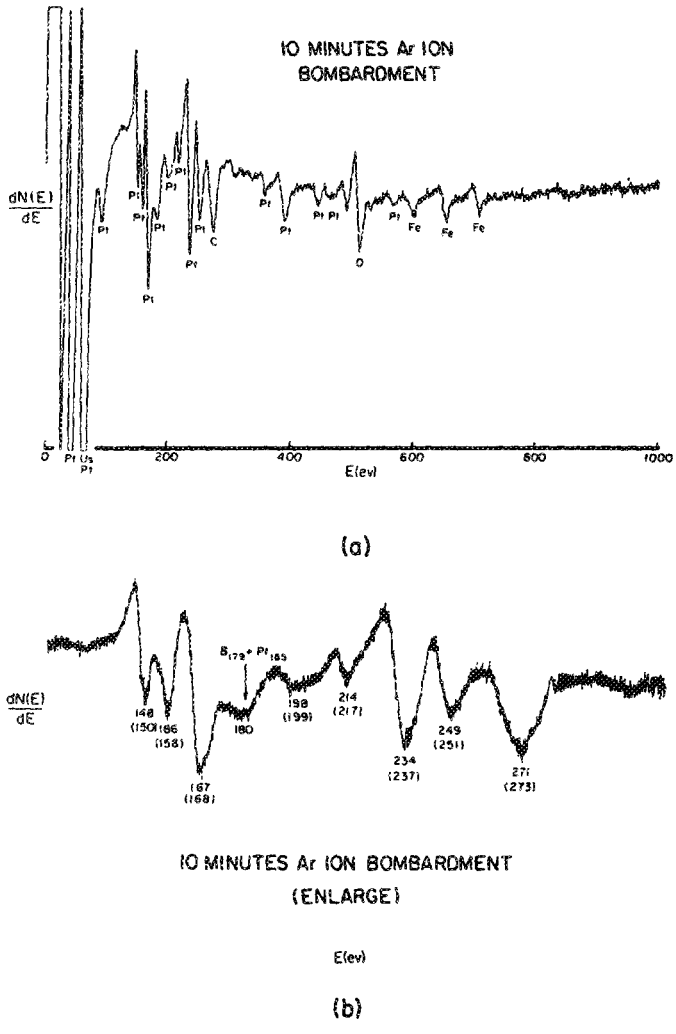

FIG. 16. AES of LMIS deposit from 10-μm emitter tip radius: (a) 10-min Ar ion bombardment, (b) same as (a), but enlarged.

perature, two phases of (Pt) and platinum-rich boron liquid alloy coexist. Therefore, the calculated stoichiometry from RBS results shown in Fig. 15 give an approximate composition of the alloy source. Bear in mind that during LMIS operation, beside droplet formation, a substantial amount of neutral platinum was also produced and cannot be detected by QMS. Figure 16(a) shows the Auger electron spectrum (AES) of ion beam deposits from a 10-μm graphite emitter tip radius on a silicon substrate. This spectrum was taken after a 10-min argon ion bombardment to remove oxide layers on the surface. One can notice platinum spectra at different Auger energies which cannot be detected with QMS. This result shows clear evidence that substantial platinum species were emitted as neutral atoms and only a few were ionized in a single or double-charged species. Note that the evidence of the boron spectrum shown in Figs. 9 and 10 are not revealed by AES shown in Fig. 16. The reason for this is that boron and platinum have very close and nonresolved Auger electron energies of 179 and 180 eV for boron and platinum, respectively. Figure 16(b) shows an expanded scale of Fig. 16(a) in order to separate the peaks so that they can be seen more clearly. Notice that the coexistence of peaks at 179 eV (B) and 180 eV (Pt) makes them indistinguishable from the platinum spectrum. Other elements notably C and Fe shown in the Auger spectrum [see Fig. 16(a)] come from the impurities, particularly for Fe. Carbon more likely comes from the emitter tip erosion during LMIS operation. The erosion is caused by the hydrostatic tension stress generated by the applied electric field which tends to pull on the liquid film covering the needle apex.

The blunting of the needle which initially had an apex radius of 10 μm has been observed with scanning electron microscopy (SEM), and is shown in Fig. 17. The emitter tip radius is almost 20 times larger than its original size. This result demonstrates that during LMIS operation, not only droplets and neutral atoms are produced but also emitter tip erosion occurs as a result of electric field stress which "pulls" on the liquid film. The evidence obtained from surface analysis clearly shows the change in alloy stoichiometry, formation of droplets, and neutral platinum atoms in the beam during LMIS operation. These experimental results have common characteristics such as those which have been explained by the hydrodynamic model LMIS proposed earlier for the uniary system.[11]

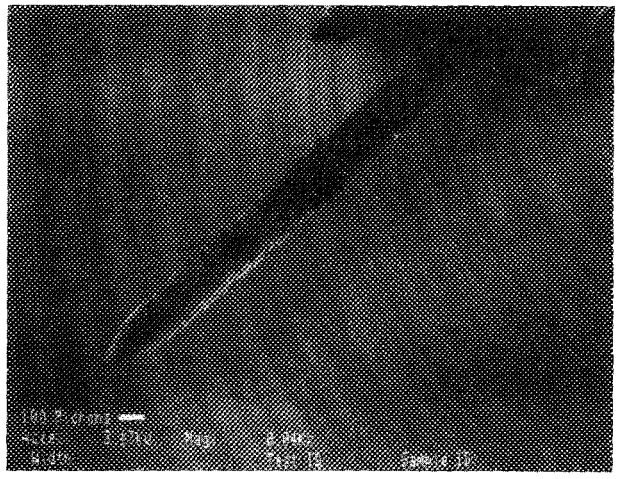

100 Microns

(a)

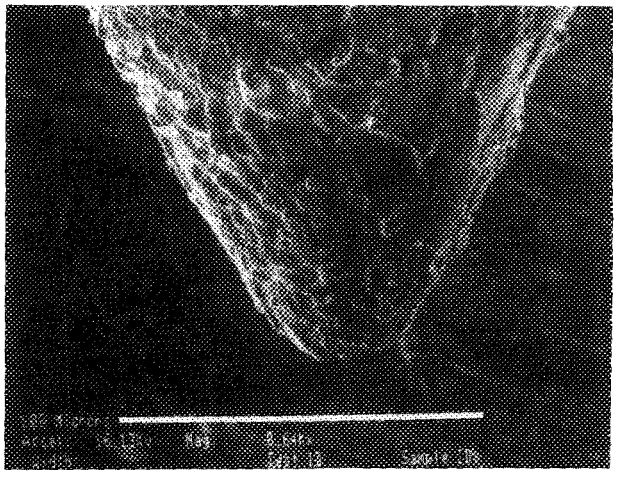

100 Microns

(b)

FIG. 17. SEM of 10-μm emitter tip after lifetime test: (a) overall needle shank, (b) detail of needle tip.

IV. CONCLUSIONS

The binary boron platinum ($Pt_{58}B_{42}$) LMIS has many characteristics in common with the hydrodynamic model of LMIS.[11] A 2.5-μm graphite emitter tip produced the most stable $^{11}B^+$ emission during its lifetime recorded up to 26 h, and the instability is less than 2%. More droplets and neutral platinum were produced with a 10-μm emitter tip radius, resulting in unstable $^{11}B^+$ ion emission. RBS results show that more boron is produced in the beam than left behind in the liquid alloy. Neutral platinum atoms were detected by AES which were not observable with QMS. This boron alloy source fulfilled six out of the seven requirements outlined as ideal criteria for boron-producing alloy sources for use in the FIB application and the criteria are based on the type of LMIS design used in this investigation.

ACKNOWLEDGMENT

The authors gratefully acknowledge support of this work by the Semiconductor Research Corporation.

[1]R. Clampitt, K. L. Aiken, and D. K. Jefferies, J. Vac. Sci. Technol. **12**, 1208 (1975).
[2]K. Gamo, T. Ukegawa, Y. Inomoto, Ki Kan Ka, and S. Namba, Jpn. J. Appl. Phys. **19**, L595 (1980).
[3]R. L. Kubena, C. Anderson, R. L. Seliger, R. Julles, and E. Stevens, J. Vac. Sci. Technol. **19**, 916 (1981).
[4]T. Ishitani, K. Uemura, and H. Tamura, Jpn. J. Appl. Phys. **23**, 33 (1984).
[5]K. Gamo, T. Ukegawa, Y. Inomoto, Y. Ochiai, and S. Namba, J. Vac. Sci. Technol. **19**, 1182 (1981).
[6]T. Ishitani, K. Uemura, S. Hosoki, T. Takagama, and H. Tamura, J. Vac. Sci. Technol. **12**, 1368 (1984).
[7]R. H. Higuchi-Rusli, K. C. Cadien, J. C. Corelli, and A. J. Steckl, J. Vac. Sci. Technol. B **5**, 190 (1987).
[8]P. D. Prewett, A. Dixon, and S. Kimura, *Proceedings of the 9th Symposium on Ion Source and Ion Assisted Technology '85, Tokyo*, edited by T.

Takasi (The Professional Group of Electron Devices, The Institute of Electrical Engineering of Japan, Tokyo, Japan, 1985), p. 585.
[9]R. H. Higuchi-Rusli, Ph.D. thesis, Rensselaer Polytechnic Institute (1986).
[10]A. Wagner, J. Vac. Sci. Technol. 6, 1871 (1979).
[11]A. Wagner, Appl. Phys. Lett. 40, 442 (1982).
[12]R. Clampitt and D. K. Jefferies, Inst. Phys. Conf. Ser. 38, 12 (1970).
[13]L. W. Swanson, G. A. Schwind, and A. E. Bell, J. Appl. Phys. 51, 3453 (1980).
[14]A. Wagner, T. Venkatesan, P. M. Petroff, and D. Bamm, J. Vac. Sci. Technol. 4, 1186 (1981).
[15]Ben Assayag and P. Sudraud, Ultramicroscopy 16, 1 (1985).
[16]W. G. Moffat, *The Handbook of Binary Phase Diagram* (General Electric, New York, 1981), Vol. 1.